arXiv:astro-ph/0305045v2 15 May 2003

Circularly Symmetric Apodization via Starshaped Masks

Robert J. Vanderbei

Operations Research and Financial Engineering, Princeton University

rvdb@princeton.edu

David N. Spergel

Astrophysical Sciences, Princeton University

dns@astro.princeton.edu

and

N. Jeremy Kasdin

Mechanical and Aerospace Engineering, Princeton University

jkasdin@princeton.edu

ABSTRACT

In Vanderbei et al. (2003), we introduced a class of shaped pupil masks, called spiderweb masks, that produce point spread functions having annular dark zones. With such masks, a single image can be used to probe a star for extrasolar planets. In this paper, we introduce a new class of shaped pupil masks that also provide annular dark zones. We call these masks starshaped masks. Given any circularly symmetric apodization function, we show how to construct a corresponding starshaped mask that has the same point-spread function (out to any given outer working distance) as obtained by the apodization.

Subject headings: Extrasolar planets, coronagraphy, Fraunhaufer optics, Hankel transform, point spread function, apodization

1. Introduction

With more than 100 extrasolar Jupiter-sized planets discovered in just the last decade, there is now great interest in discovering and characterizing Earthlike planets. To this end,

NASA is planning to launch a space-based telescope, called the *Terrestrial Planet Finder (TPF)*, sometime in the middle of the next decade. This telescope, which will ultimately be either an interferometer or a coronagraph, will be specifically designed for high-contrast imaging. Earlier studies (Brown et al. (2002)) indicate that a 4m class coronagraph ought to be able to discover about 50 extrasolar Earth-like planets if the telescope can provide contrast of 10^{-10} at a separation of $3\lambda/D$ and that a 4×10m class telescope ought to be able to discover about 150 such planets if it can provide the same contrast at a separation of $4\lambda/D$.

One of the most promising design concepts for high-contrast imaging is to use pupil masks for diffraction control. Early work in this direction (see Brown et al. (2002); Spergel (2000); Kasdin et al. (2002, 2003)) has focused on optimizing masks that are not rotationally symmetric and thus provide the desired contrast only in a narrow annular sector around a star, but at fairly high throughput. A full investigation of a given star then requires multiple images where the mask is rotated between the images so as to image all around the star. In a recent paper (Vanderbei et al. (2003)), we proposed a new class of rotationally symmetric pupil masks, which are attractive because they do not require rotation to image around a star. Such masks consist of concentric rings supported by many ultra-thin pie-shaped spiders. We call these masks *spiderweb* masks. We showed that they can provide the desired contrast with a reasonable amount of light throughput.

In this paper, we consider a similar family of binary masks. These masks consist only of spiders—there are no concentric rings. Instead, the desired contrast is obtained by carefully controlling the width of the spiders as a function of radius. We call these masks *starshaped* masks since the resulting designs look like many-pointed stars.

The paper is organized as follows. In the next section, we briefly review the relationship between pupil-plane apodization and the corresponding image-plane electric field and point-spread function. Then in Section 3, we show how to make starshape binary masks for which the first term in a Bessel expansion of the electric field matches the corresponding electric field associated with any given apodization. We show that for a sufficiently large number of star-points, the remaining terms have negligible contribution to the electric field in the annulus of interest. Finally, in Section 4 we show how to compute various "optimal" apodizations. In particular, we show that the best of these optimal apodizations is zero-one valued and in fact corresponds to the optimal spiderweb masks presented in Vanderbei et al. (2003).

2. Apodization

The image-plane electric field produced by an on-axis point source and an apodized aperture defined by a circularly-symmetric apodization function $A(\sqrt{x^2+y^2})$ is given by

$$E(\xi,\zeta) = \iint_S e^{-2\pi i(x\xi+y\zeta)} A\left(\sqrt{x^2+y^2}\right) dxdy, \tag{1}$$

where

$$S = \{(x,y):\ 0 \le r(x,y) \le 1/2,\ \theta(x,y) \in [0,2\pi]\}, \tag{2}$$

and $r(x,y)$ and $\theta(x,y)$ denote the polar coordinates associated with point (x,y). Here, and throughout the paper, x and y denote coordinates in the pupil plane measured in units of the aperature D and ξ and ζ denote angular (radian) deviations from on-axis measured in units of wavelength over aperture (λ/D) or, equivalently, physical distance in the image plane measured in units of focal-length times wavelength over aperture $(f\lambda/D)$.

For circularly-symmetric apodizations, it is convenient to work in polar coordinates. To this end, let r and θ denote polar coordinates in the pupil plane and let ρ and ϕ denote the image plane coordinates:

$$\begin{array}{rclcrcl} x &=& r\cos\theta & & \xi &=& \rho\cos\phi \\ y &=& r\sin\theta & & \zeta &=& \rho\sin\phi. \end{array} \tag{3}$$

Hence,

$$\begin{aligned} x\xi + y\zeta &= r\rho(\cos\theta\cos\phi + \sin\theta\sin\phi) && (4)\\ &= r\rho\cos(\theta-\phi). && (5) \end{aligned}$$

The electric field in polar coordinates depends only on ρ and is given by

$$\begin{aligned} E(\rho) &= \int_0^{1/2}\int_0^{2\pi} e^{-2\pi i r\rho\cos(\theta-\phi)} A(r) r d\theta dr, && (6)\\ &= 2\pi \int_0^{1/2} J_0(2\pi r\rho) A(r) r dr, && (7) \end{aligned}$$

where J_0 denotes the 0-th order Bessel function of the first kind. Note that the mapping from apodization function A to electric field E is linear. Furthermore, the electric field in the image plane is real-valued (because of symmetry).

The *point spread function* (psf) is the square of the electric field in the image plane. The contrast requirement is that the psf in the dark region be 10^{-10} of what it is at its center. Because the electric field is real-valued, it is convenient to express the contrast requirement in terms of it rather than the psf, resulting in a field requirement of $\pm 10^{-5}$.

A second requirement is high throughput. The most natural measure of throughput is the area under the main lobe of the psf:

$$\mathcal{T}_{\text{Airy}} = \int_0^{\rho_{\text{iwd}}} E^2(\rho) 2\pi\rho d\rho, \tag{8}$$

where ρ_{iwd} denotes the location of the first null of the psf. We call this measure the *Airy-throughput*. Two other measures of throughput are relevant to our discussion. The *total throughput* of an apodization is the integral of the psf over the entire image plane. By Parseval's theorem, the total throughput is also the integral of the square of the apodization:

$$\mathcal{T}_{\text{total}} = \int_0^{\infty} E^2(\rho) 2\pi\rho d\rho = \int_0^{1/2} A^2(r) 2\pi r dr. \tag{9}$$

The electric field at $\rho = 0$,

$$E(0) = \int_0^{1/2} A(r) 2\pi r dr, \tag{10}$$

provides another measure of the "central" throughput of the apodization, since its square is the peak throughput density at the center of the Airy disk. If $A()$ is zero-one valued, then the apodization can be realized as a mask. In this case, $E(0)$ is precisely the open area of the mask (and is also the total-throughput). For this reason, we call $E(0)$ the *pseudo-area* of the apodization even when the apodization is not zero-one valued.

3. Starshape Masks

In this section, we study binary mask approximations to any apodized pupil. The masks we consider are *starshaped*—see Figure 1. The opening in an N-point starshaped mask can be described mathematically by a set S given by:

$$S = \{(x, y) : \ 0 \le r(x, y) \le 1/2, \ \theta(x, y) \in \Theta\}, \tag{11}$$

$$\Theta = \bigcup_{n=0}^{N-1} \left[\frac{2\pi n}{N} + \frac{\alpha(r)}{2}, \frac{2\pi(n+1)}{N} - \frac{\alpha(r)}{2} \right], \tag{12}$$

where $\alpha(r)$ denotes the width in radians of a "vane" and the notation $[a, b]$ denotes the interval on the real line from a to b. Note that the shape of each point of the star is determined by the function $\alpha(r)$. Our aim is to determine choices for this function that will yield an image-plane psf matching the psf corresponding to any given apodization.

The electric field, expressed in polar coordinates, associated with starshape mask S is given by

$$E(\rho, \phi) = \iint_S e^{-2\pi i r\rho\cos(\theta-\phi)} r dr d\theta. \tag{13}$$

The integral in equation (13) can be expressed in terms of Bessel functions using the Jacobi-Anger expansion (see, e.g., Arfken and Weber (2000) p. 681):

$$e^{ix\cos\theta} = \sum_{m=-\infty}^{\infty} i^m J_m(x) e^{im\theta}. \tag{14}$$

Substituting into (13), we get:

$$\begin{aligned} E(\rho, \phi) &= \iint_S \sum_m i^m J_m(-2\pi r\rho) e^{im(\theta-\phi)} r dr d\theta & (15)\\ &= \int_0^{1/2} \sum_m i^m J_m(-2\pi r\rho) e^{-im\phi} \left(\int_\Theta e^{im\theta} d\theta \right) r dr & (16) \end{aligned}$$

The integral over Θ is easy to compute:

$$\begin{aligned} \int_\Theta e^{im\theta} d\theta &= \sum_{n=0}^{N-1} \int_{\frac{2\pi n}{N}+\frac{\alpha(r)}{2}}^{\frac{2\pi(n+1)}{N}-\frac{\alpha(r)}{2}} e^{im\theta} d\theta & (17)\\ &= \begin{cases} 2\pi - N\alpha(r) & m = 0 \\ -\frac{2}{j}\sin(jN\frac{\alpha(r)}{2}) & m = jN,\ j \neq 0 \\ 0 & \text{otherwise.} \end{cases} & (18) \end{aligned}$$

Substituting this result into (13), yields

$$\begin{aligned} E(\rho, \phi) &= \int_0^{1/2} J_0(-2\pi r\rho)(2\pi - N\alpha(r)) r dr & (19)\\ &\quad - \sum_{j\neq 0} \int_0^{1/2} i^{jN} J_{jN}(-2\pi r\rho) e^{-ijN\phi} \frac{2}{j} \sin\left(jN\frac{\alpha(r)}{2} \right) r dr. & (20) \end{aligned}$$

Lastly, suppose that N is even and use the fact that $J_{-m}(x) = J_m(-x) = (-1)^m J_m(x)$ to get the following expansion for the electric field:

$$E(\rho,\phi) = 2\pi \int_0^{1/2} J_0(2\pi r\rho)(1-\frac{N}{2\pi}\alpha(r))rdr \tag{21}$$

$$-4\sum_{j=1}^{\infty}\int_0^{1/2} J_{jN}(2\pi r\rho)\cos(jN(\phi-\pi/2))\frac{1}{j}\sin(jN\frac{\alpha(r)}{2})rdr. \tag{22}$$

The first term, involving the integral of J_0, is identical to the formula for the electric field for an apodized aperture with

$$A(r) = 1 - \frac{N}{2\pi}\alpha(r). \tag{23}$$

Hence, by putting

$$\alpha(r) = \frac{2\pi}{N}\left(1 - A(r)\right), \tag{24}$$

we can make the first term match any circularly symmetric apodization.

Furthermore, for large N, the effect of the higher-order Bessel terms becomes negligible for small ρ. Indeed, for $z \le \sqrt{4(m+1)}$,

$$0 \le J_m(z) \le \frac{(z/2)^{m+1}}{(m+1)!}, \tag{25}$$

(which itself follows easily from the alternating Taylor series expansion of the m-th Bessel function: $J_m(z) = \sum_{l=0}^{\infty}(-1)^l(z/2)^{2l+m}/(l!(m+l)!)$). From this we use the Schwarz inequality to estimate the magnitude of the effect of the higher-order terms:

$$\begin{aligned}\left| \quad 4\sum_{j=1}^{\infty}\int_0^{1/2} J_{jN}(2\pi r\rho)\cos(jN(\phi-\pi/2))\frac{1}{j}\sin(jN\frac{\alpha(r)}{2})rdr \quad \right| \\ \le \frac{1}{2}\sum_{j=1}^{\infty} J_{jN}(\pi\rho_{\rm owd}) \\ \le \frac{1}{2}\sum_{j=1}^{\infty}\frac{1}{(jN+1)!}\left(\frac{\pi\rho_{\rm owd}}{2}\right)^{jN+1},\end{aligned} \tag{26}$$

for $\rho_{\rm owd} \le \sqrt{4(N+1)}/\pi$. Since the last bound is dominated by $e^{\pi\rho_{\rm owd}/2}/2$, it follows from the dominated convergence theorem that this last bound tends to zero as N tends to infinity.

The convergence to zero of the terms in the sum on j is very fast. In fact, if N is set large enough such that $\max_{0\le z\le \pi\rho_{\rm owd}} J_N(z) \le 10^{-5}$, then the $j=1$ term dominates the sum of all the higher-order terms and is itself dominated by the J_0 term. Figure 2 shows a plot of J_{50}, J_{100}, and J_{150}. These three Bessel functions first reach 10^{-5} at $z = 35.2$, 81.0, and 128.1, respectively. This suggests that a contrast level of 10^{-10} can be preserved out to $35\lambda/D$ using about $N = 50$ vanes, out to $80\lambda/D$ using about $N = 100$ vanes, and out to $120\lambda/D$ using about $N = 150$ vanes. These estimates ignore the contribution from higher-order terms. In practice, more vanes are required to preserve the desired contrast level to these outer working distances.

Within the discovery zone, the electric fields resulting from the apodization and the starshaped mask agree. Hence, the Airy-thoughputs and pseudo-areas also agree. But, the total throughput for the mask is larger, often by a factor of about two. Indeed, the total throughput of the apodization is

$$\mathcal{T}_{\rm total,apod} = \int_0^{1/2} A(r)^2 2\pi r dr \tag{27}$$

whereas, from (12) and (23), it follows that the total throughput of the mask is

$$\mathcal{T}_{\rm total,mask} = \iint_S r dr d\theta = \int_0^{1/2} A(r) 2\pi r dr \ge \mathcal{T}_{\rm apod} \tag{28}$$

(the inequality holds because $0 \le A(r) \le 1$). So, the mask lets about twice as much light through but the extra light is necessarily concentrated outside the outer working distance.

4. Apodizations Optimized for TPF

There has been much interest in using apodized pupils to achieve high-contrast imaging, especially recently in the context of TPF studies: see e.g. Jacquinot and Roizen-Dossier (1964); Indebetouw (1990); Watson et al. (1991); Nisenson and Papaliolios (2001).

The simplest optimization problem involves maximizing the pseudo-area subject to contrast constraints. It can be formulated as an infinite dimensional linear optimization problem:

$$\begin{array}{lll} \text{maximize} & \int_0^{1/2} A(r) 2\pi r dr & \\ \text{subject to} & -10^{-5}E(0) \le E(\rho) \le 10^{-5}E(0), & \rho_{\rm iwd} \le \rho \le \rho_{\rm owd}, \\ & 0 \le A(r) \le 1, & 0 \le r \le 1/2, \end{array} \tag{29}$$

where $\rho_{\rm iwd}$ denotes a fixed *inner working distance* and $\rho_{\rm owd}$ a fixed *outer working distance*. Discretizing the sets of r's and ρ's and replacing the integrals with their Riemann sums, problem (29) is approximated by a finite dimensional linear programming problem, which can be solved to a high level of precision (see, e.g., Vanderbei (2001)). The numerical solution to this problem reveals that the optimal solution is zero-one valued. That is, the optimal apodization is, in fact, a mask consisting of concentric rings.

A second optimization problem involves maximizing total-throughput:

$$\begin{array}{lll} \text{maximize} & \int_0^{1/2} A(r)^2 2\pi r dr & \\ \text{subject to} & -10^{-5}E(0) \le E(\rho) \le 10^{-5}E(0), & \rho_{\rm iwd} \le \rho \le \rho_{\rm owd}, \\ & 0 \le A(r) \le 1, & 0 \le r \le 1/2. \end{array} \tag{30}$$

An empirical observation is that this more difficult optimization problem also proves to be tractible and, in all cases tried, provides the same optimal apodization as was obtained by maximizing pseudo-area.

The solution obtained for $\rho_{\rm iwd} = 4$ and $\rho_{\rm owd} = 60$ is shown in Figure 3. The throughput is 17.9% and, since it is a mask, its pseudo-area is the same. Its Airy-thoughput is 9.37%. (Note: all results are reported as a percentage of the largest possible value which would result from a completely open aperture. That is, all throughputs are divided by the area $\pi(1/2)^2$ and labeled as percentages.)

The starshaped mask associated with this "apodization" is precisely the same concentric-ring mask independent of the number of star points chosen, since the star points disappear entirely. Of course, this mask cannot be manufactured as the concentric rings need some means of support. If one imposes an upper bound on A in (29) that is strictly less than unity, then one obtains a supportable mask with slightly reduced throughput (the amount depending on the upper bound chosen). Such a mask is exactly the spiderweb mask studied in Vanderbei et al. (2003).

In this paper, we are interested in smooth apodizations. To this end, we add seemingly artificial smoothness constraints to the optimization problem. Motivated by the fact that optimal apodizations look qualitatively like a Gaussian function, we impose smoothness constraints that correspond to the following conditions:

$$\log(A)' \le 0 \tag{31}$$

$$\log(A)'' \le 0. \tag{32}$$

The resulting max-pseudo-area optimization problem is:

$$\begin{array}{lrlll} \text{maximize} & \int_0^{1/2} A(r) 2\pi r dr & & & \\ \text{subject to} & -10^{-5}E(0) \leq & E(\rho) & \leq 10^{-5}E(0), & \rho_{\rm iwd} \leq \rho \leq \rho_{\rm owd}, \\ & 0 \leq & A(r) & \leq 1, & 0 \leq r \leq 1/2, \\ & & A'(r) & \leq 0, & 0 \leq r \leq 1/2, \\ & & A(r)A''(r) & \leq A'(r)^2, & 0 \leq r \leq 1/2. \end{array} \tag{33}$$

The solution obtained for $\rho_{\rm iwd} = 4$ and $\rho_{\rm owd} = 60$ is shown in Figure 4. The total-throughput for this apodization is 9.12%. Its Airy-throughput is 9.09% and its pseudo-area is 17.39%. The psf's for the corresponding starshape masks with 20 and 150 point stars are shown in Figure 5. Other apodizations satisfying the smoothness constraints (such as the generalized prolate spheroidal apodization discussed in the next subsection), being less optimal, must necessarily have even smaller throughputs.

There is great interest in reducing the inner working distance to something less than $\rho_{\rm iwd} = 4$, as this would increase the number of likely target stars for TPF. Smaller inner working distances can be achieved if if one is willing to accept a smaller outer working distance too (di Francia (1952)). Unfortunately, a small reduction in inner working distance requires a large reduction in outer working distance so that very quickly the discovery zone becomes a very narrow annulus. For example, the solution obtained for $\rho_{\rm iwd} = 3$ and $\rho_{\rm owd} = 4.25$ is shown in Figure 6. The total-throughput for this apodization is 7.7%. Its Airy-throughput is 7.6% and its pseudo-area is 20.0%. The 50-point starshaped mask associated with this apodization is shown in Figure 7.

Optimizing pseudo-area or total-throughput are really just simple surrogates for the true objective, which is to minimize integration time. Burrows (1994) has shown that maximizing *sharpness* translates directly into minimizing the integration time required to reach a specified signal to noise ratio. However, it seems to us that optimizing sharpness is beyond the capabilities of our optimization tools. Hence, we optimize the simple surrogates and reserve sharpness calculations for later comparing various designs.

4.1. The Generalized Prolate Spheroidal Apodization

Generalized prolate spheroidal wave functions were first introduced by Slepian (1965) as a way to apodize a circularly symmetric aperture so as to concentrate as much light as possible into a central Airy disk. In the context of TPF, the generalized prolate spheroidal wave function has been popularly viewed as providing an optimal apodization (see, e.g., Kasdin et al. (2003); Aime et al. (2001); Gonsalves and Nisenson (2003)). However, in truth,

it is an optimal solution to the following slightly different optimization problem[1]:

$$\begin{aligned} &\text{minimize} \quad \int_{\rho_{\text{iwd}}}^{\infty} E(\rho)^2 d\rho \\ &\text{subject to} \quad A(0) = 1. \end{aligned} \tag{34}$$

The generalized prolate spheroidal apodization computed using $\rho_{\text{iwd}} = 4$ gives 8.3% total-throughput. The Airy-throughput is essentially the same. The pseudo-area is 15.9%. The apodization and corresponding psf are shown in Figure 8. At the expense of Airy-throughput (8.3% vs. 9.1%) and slight violation of the contrast in the first few diffraction rings, it has better than needed contrast throughout most of a larger than needed dark zone.

The throughputs for the apodizations discussed in this section are summarized in Table 1.

5. Final Remarks

Some TPF concepts involve an elliptical pupil geometry since this might provide a means to achieve improved angular resolution in realizable rocket fairings. The designs presented in this paper are given in unitless variables. When re-unitizing, a different scale can be used for the x and y directions. In this way, these designs can be applied directly to elliptical pupils. Of course, the high-contrast region of the psf will also be elliptical with the short axis of the psf corresponding to the long axis of the pupil.

There are two parts to TPF: discovery and characterization. Discovery refers to the simple act of looking for exosolar planets. Characterization refers to the process of learning as much as possible about specific planets after they have been discovered. The masks presented here are intended primarily for discovery since a single exposure with these masks can discover a planet in any orientation relative to its star. However, once a planet is found and its orientation is known, some of the asymmetric masks presented in previous papers should be used for photometry and spectroscopy as they have significantly higher single-exposure throughput.

An alternative to pupil masks is to use a traditional coronagraph, which consists of an image plane mask followed by a Lyot stop in a reimaged pupil plane. Recently, Kuchner

[1]Slepian actually formulated it as an equivalent unconstrained optimization problem: $\max \int_0^{\rho_{\text{iwd}}} E(\rho)^2 d\rho / \int_0^{\infty} E(\rho)^2 d\rho$.

and Traub (2002) have developed band-limited image-plane masks that achieve the desired contrast to within $3\lambda/D$. A potential drawback of this approach is its sensitivity to pointing accuracy. Nonetheless, it appears very promising. In the future, we plan to consider combining pupil masks with image masks and Lyot stops to make a hybrid design that hopefully will provide a design achieving the desired contrast with an even smaller inner working distance and perhaps higher throughput.

In this paper we have only considered scalar electric fields. We leave the important and more complex issue of how to treat vector electric fields, i.e. polarized light, to future work.

Acknowledgements. We would like to express our gratitude to our colleagues on the Ball Aerospace and Technology TPF team. We benefited greatly from the many enjoyable and stimulating discussions. This work was partially performed for the Jet Propulsion Laboratory, California Institute of Technology, sponsored by the National Aeronautics and Space Administration as part of the TPF architecture studies and also under contract number 1240729. The first author received support from the NSF (CCR-0098040) and the ONR (N00014-98-1-0036).

REFERENCES

C. Aime, R. Soummer, and A. Ferrari. Interferometric apodization of rectangular apertures. *Astronomy and Astrophysics*, 379(2):697–707, 2001.

G.B. Arfken and H.J. Weber. *Mathematical Methods for Physicists*. Harcourt/Academic Press, 5th edition, 2000.

R. A. Brown, C. J. Burrows, S. Casertano, M. Clampin, D. Eggets, E.B. Ford, K.W. Jucks, N. J. Kasdin, S. Kilston, M. J. Kuchner, S. Seager, A. Sozzetti, D. N. Spergel, W. A. Traub, J. T. Trauger, and E. L. Turner. The 4-meter space telescope for investigating extrasolar earth-like planets in starlight: TPF is HST2. In *Proceedings of SPIE: Astronomical Telescopes and Instrumentation*, number 14 in 4860, 2002.

C. Burrows. Signal to noise ratio in background limited telescopic images. Technical report, STSI, 1994.

G. Toraldo di Francia. Super-gain antenna and optical resolving power. *Serie IX del Nuovo Cimento*, Supplemento al Volume IX(3), 1952.

R. Gonsalves and P. Nisenson. Calculation of an optimized telescope apodizer for terrestrial planet finder coronagraphic telescope. *Publications of the Astronomical Society of the Pacific*, 2003. To appear.

G. Indebetouw. Optimal apodizing properties of gaussian pupils. *Journal of Modern Optics*, 37(7):1271–1275, 1990.

P. Jacquinot and B. Roizen-Dossier. Apodisation. *Progess in Optics*, 3:29–186, 1964.

N.J. Kasdin, R.J. Vanderbei, D.N. Spergel, and M.G. Littman. Optimal Shaped Pupil Coronagraphs for Extrasolar Planet Finding. In *Proceedings of SPIE Conference on Astronomical Telescopes and Instrumentation*, number 44 in 4860, 2002.

N.J. Kasdin, R.J. Vanderbei, D.N. Spergel, and M.G. Littman. Extrasolar Planet Finding via Optimal Apodized and Shaped Pupil Coronagraphs. *Astrophysical Journal*, 582: 1147–1161, 2003.

M. J. Kuchner and W. A. Traub. A coronagraph with a band-limited mask for finding terrestrial planets. *The Astrophysical Journal*, (570):900+, 2002.

P. Nisenson and C. Papaliolios. Detection of earth-like planets using apodized telescopes. *The Astrophysical Journal*, 548(2):L201–L205, 2001.

D. Slepian. Analytic solution of two apodization problems. *Journal of the Optical Society of America*, 55(9):1110–1115, 1965.

D. N. Spergel. A new pupil for detecting extrasolar planets. *astro-ph/0101142*, 2000.

R.J. Vanderbei. *Linear Programming: Foundations and Extensions*. Kluwer Academic Publishers, 2nd edition, 2001.

R.J. Vanderbei, D.N. Spergel, and N.J. Kasdin. Spiderweb Masks for High Contrast Imaging. *Astrophysical Journal*, 2003. To appear.

S. M. Watson, J. P. Mills, S. L. Gaiser, and D. J. Diner. Direct imaging of nonsolar planets with infrared telescopes using apodized coronagraphs. *Applied Optics*, 30(22):3253–3260, 1991.

This preprint was prepared with the AAS LaTeX macros v5.0.

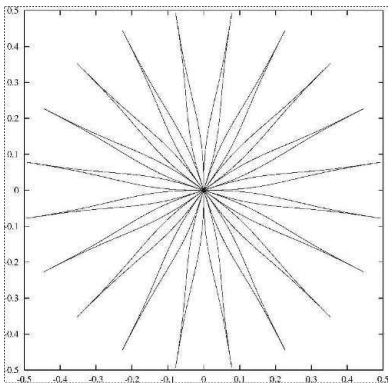

Fig. 1.— A 20-point starshape mask corresponding to the apodization shown in Figure 4.

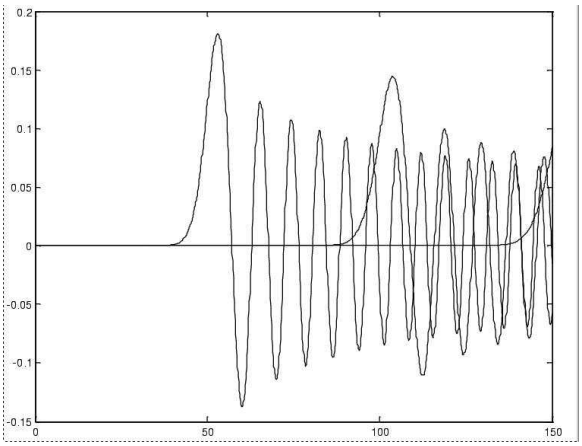

Fig. 2.— The Bessel functions J_{50}, J_{100}, and J_{150}. They first reach 10^{-5} at 35.2, 81.0, and 128.1, respectively.

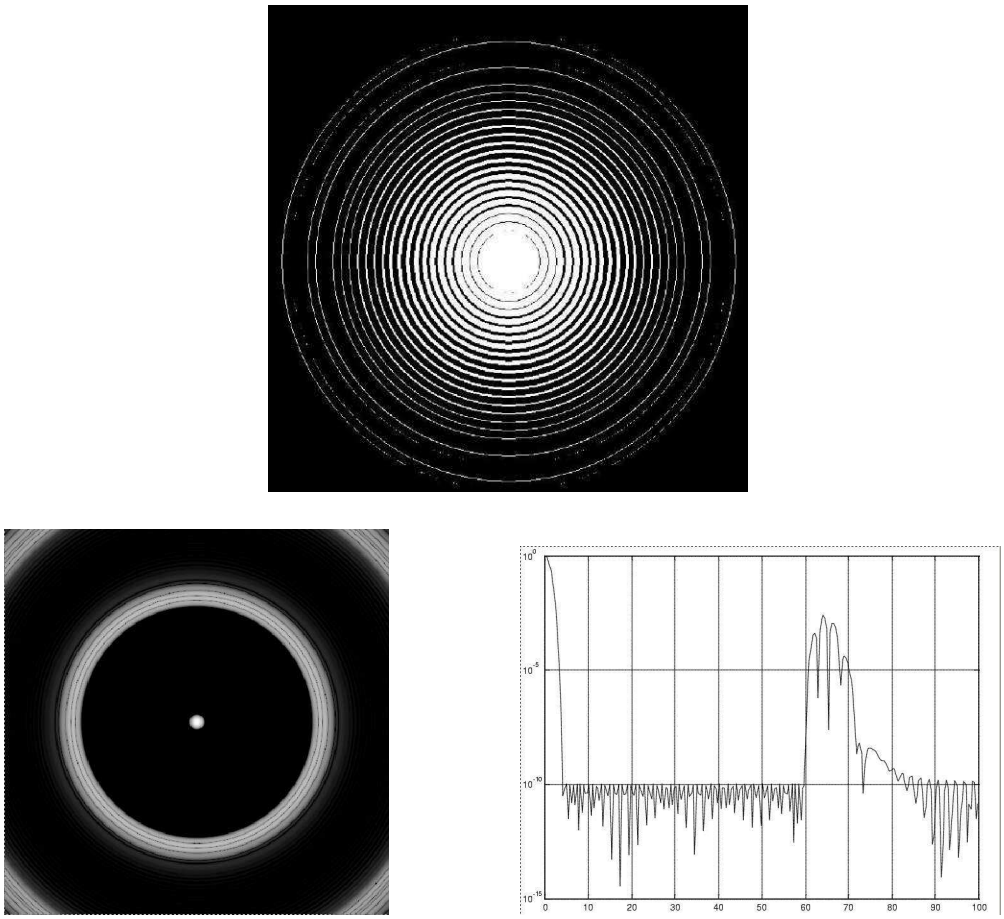

Fig. 3.— *Top.* A concentric-ring mask designed to provide high-contrast, 10^{-10}, from $\lambda/D = 4$ to $\lambda/D = 60$. Total throughput and pseudo-area are 17.9%. Airy throughput is 9.37%. *Bottom.* The associated psf.

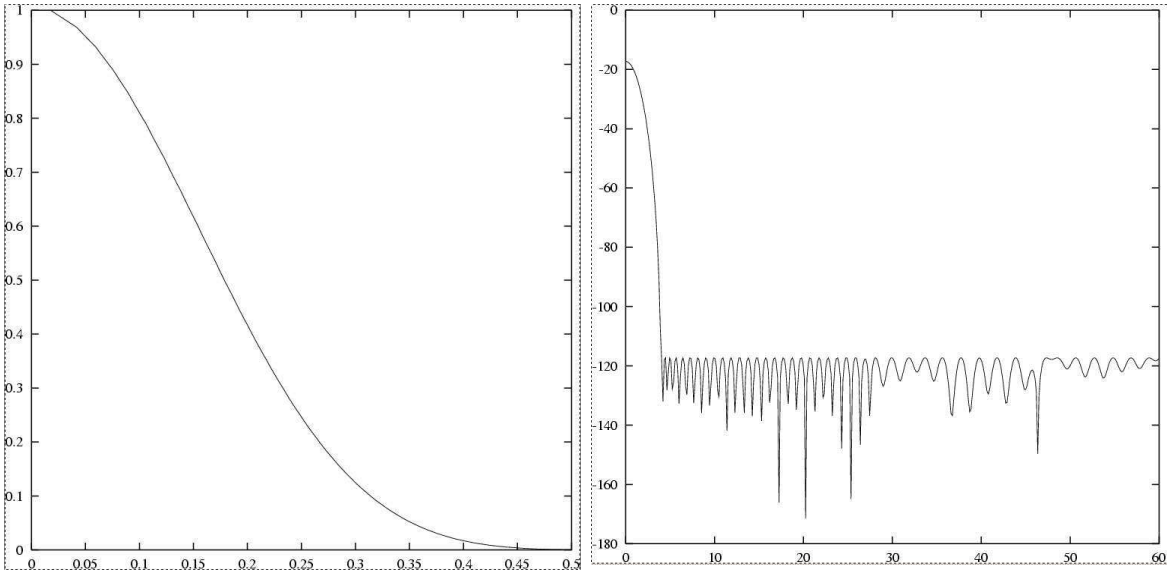

Fig. 4.— The optimal apodization for $\rho_{\rm iwd} = 4$ and $\rho_{\rm owd} = 60$ and the associated psf. Total throughput is 9.12%. Pseudo-area is 17.39%. Airy-throughput is 9.09%.

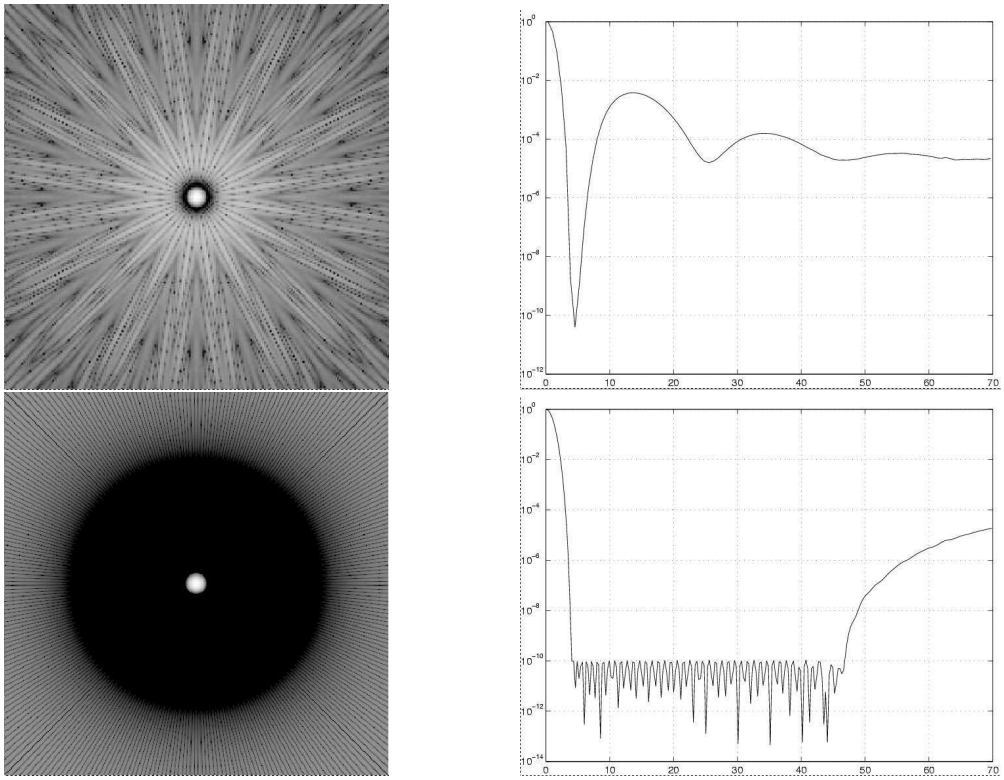

Fig. 5.— Psf's for starshape mask in associated with apodization shown in Figure 4. *Top Row.* 20-point star. *Second Row.* 150-point star.

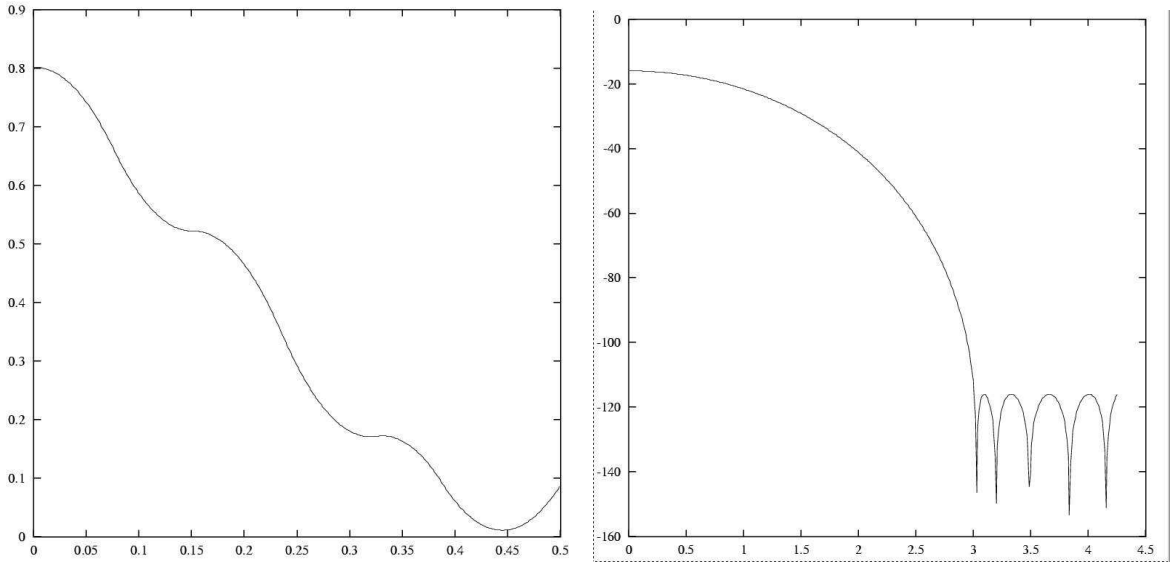

Fig. 6.— The optimal apodization for $\rho_{\rm iwd} = 3$ and $\rho_{\rm owd} = 4.25$ and the associated psf. Total throughput is 7.7%. Pseudo-area is 20.0%. Airy-throughput is 7.6%.

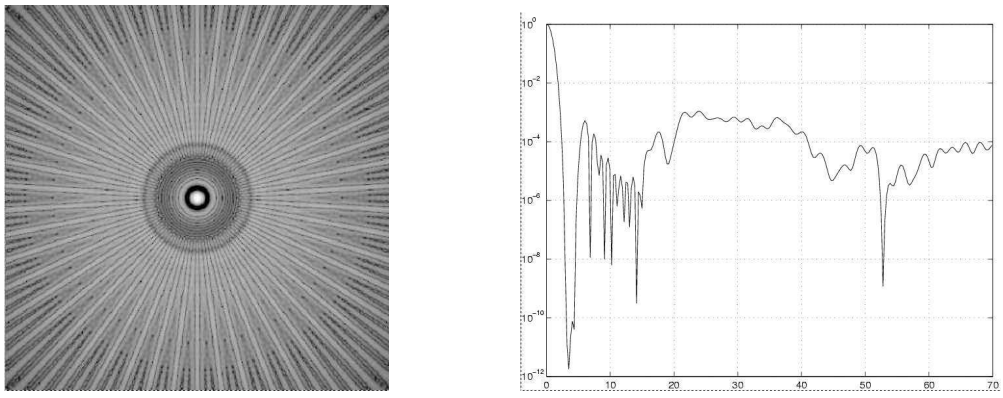

Fig. 7.— Psf's for starshape mask in associated with apodization shown in Figure 6. 50-point star.

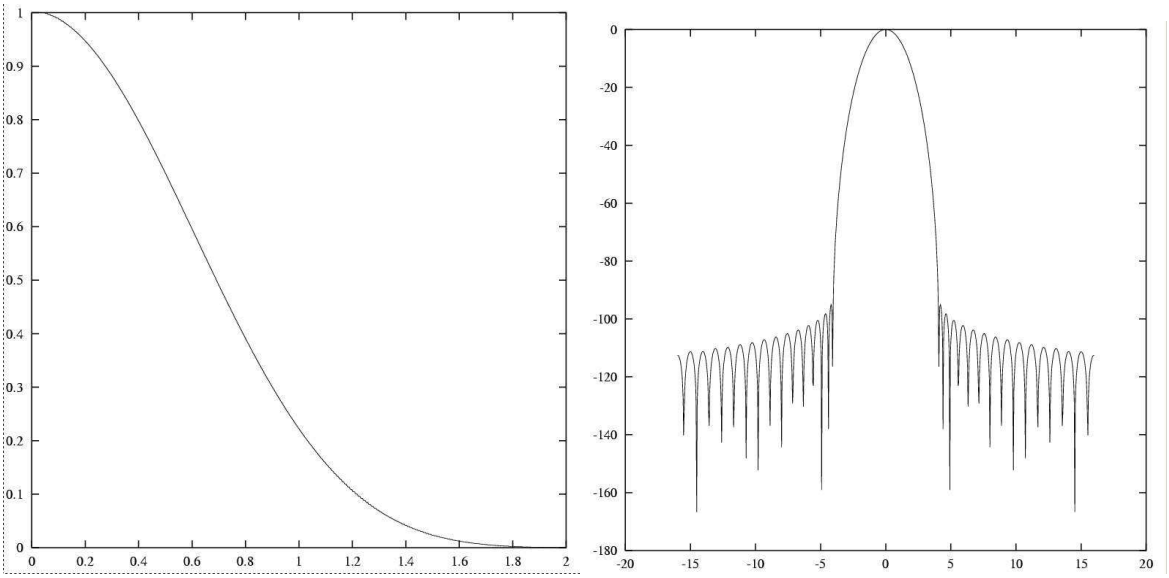

Fig. 8.— *Left.* The generalized prolate spheroidal apodization computed using $\rho_{\rm iwd} = 4$. Total throughput and Airy-throughput agree and are equal to 8.52%. The pseudo-area is 16.28%. *Right.* The associated psf.

	Smooth?	ρ_{iwd}	ρ_{owd}	$\mathcal{T}_{\rm total}$	$\mathcal{T}_{\rm Airy}$	$E(0)$
Figure 3	No	4	60	17.9	9.37	17.9
Figure 4	Yes	4	60	9.12	9.09	17.39
Figure 6	Yes	3	4.25	7.7	7.6	20.0
Figure 8	Yes	4	60	8.34	8.34	15.94

Table 1: Summary of the throughput results for the specific apodizations considered.